

1 **Cell wall damage reveals spatial flexibility in peptidoglycan synthesis and a non-**
2 **redundant role for RodA in mycobacteria**

3 Running title: Spatial flexibility in mycobacterial cell wall synthesis

4
5 Emily S. Melzer¹, Takehiro Kado¹, Alam García-Heredia^{2,3}, Kuldeepkumar Ramnaresh Gupta⁴,
6 Xavier Meniche⁵, Yasu S. Morita^{1,2}, Christopher M. Sasseti⁵, E. Hesper Rego⁴, M. Sloan
7 Siegrist^{1,2,#}

8
9 **Affiliations:**

10 ¹Department of Microbiology, University of Massachusetts, Amherst, MA 01003, USA

11 ²Molecular and Cellular Biology Graduate Program, University of Massachusetts
12 Amherst, MA 01003

13 ³Department of Biology, Massachusetts Institute of Technology, Cambridge, MA 02139

14 ⁴Department of Microbial Pathogenesis, Yale University School of Medicine, New
15 Haven, CT 06519

16 ⁵Department of Microbiology and Physiological Systems, University of Massachusetts
17 Medical School, Worcester, MA 01655

18
19 Correspondence: M.S. Siegrist (siegrist@umass.edu)

20
21 Research was supported by funds from the National Institutes of Health (NIH) under
22 awards funding R21 AI144748, R01 AI148255, and DP2 AI138238. ESM was supported
23 by NIH T32 GM008515 administered to the Chemistry Biology Interface Program at the

24 University of Massachusetts Amherst. We are grateful to Ms. Emily Bechtold for
25 technical assistance.

26

27 **Importance**

28 Peptidoglycan synthesis is a highly successful target for antibiotics. The pathway has
29 been extensively studied in model organisms under laboratory-optimized conditions. In
30 natural environments, bacteria are frequently under attack. Moreover the vast majority
31 of bacterial species are unlikely to fit a single paradigm because of differences in growth
32 mode and/or envelope structure. Studying cell wall synthesis under non-optimal
33 conditions and in non-standard species may improve our understanding of pathway
34 function and suggest new inhibition strategies. *Mycobacterium smegmatis*, a relative of
35 several notorious human and animal pathogens, has an unusual polar growth mode and
36 multi-layered envelope. In this work we challenged *M. smegmatis* with cell wall-
37 damaging enzymes to characterize the roles of cell wall-building enzymes when the
38 bacterium is under attack.

39 **Abstract**

40

41 Cell wall peptidoglycan is a heteropolymeric mesh that protects the bacteria from
42 internal turgor and external insults. In many rod-shaped bacteria, peptidoglycan
43 synthesis for normal growth is achieved by two distinct pathways: the Rod complex,
44 comprised of MreB, RodA and a cognate class B PBP, and the class A PBPs. In

45 contrast to laterally-growing bacteria, pole-growing mycobacteria do not encode an
46 MreB homolog and do not require SEDS protein RodA for *in vitro* growth. However,
47 RodA contributes to survival of *Mycobacterium tuberculosis* in some infection models,
48 suggesting that the protein could have a stress-dependent role in maintaining cell wall
49 integrity. Under basal conditions, we find here that the subcellular distribution of RodA
50 largely overlaps with that of the aPBP PonA1, and that both RodA and the aPBPs
51 promote polar peptidoglycan assembly. Upon cell wall damage, RodA fortifies *M.*
52 *smegmatis* against lysis and, unlike aPBPs, contributes to a shift in peptidoglycan
53 assembly from the poles to the sidewall. Neither RodA nor PonA1 relocate; instead,
54 the redistribution of nascent cell wall parallels that of peptidoglycan precursor synthase
55 MurG. Our results support a model in which mycobacteria balance polar growth and
56 cell-wide repair via spatial flexibility in precursor synthesis and extracellular insertion.

57

58 **Introduction**

59 Bacterial cell wall peptidoglycan is required for viability in most species under most
60 conditions (1). Although peptidoglycan synthesis has been extensively studied, much of
61 this work has been done under idealized growth conditions that do not reflect the variety
62 of stressors found in the natural environment. Outside of the laboratory, the bacterial
63 cell wall is under constant attack. In virtually all environments, competitors, predators,
64 and unwilling hosts challenge bacteria with peptidoglycan-hydrolyzing enzymes (1-5).
65 However, mechanisms to counteract cell wall damage are poorly defined. Studying
66 peptidoglycan synthesis and remodeling under non-optimal stress conditions may lead

67 to a better understanding of pathogenesis and ecologically-relevant pathways and
68 interactions.

69

70 In laterally-growing, rod-shaped organisms like *Escherichia coli* and *Bacillus subtilis*, the
71 combined activity of two distinct peptidoglycan polymerization pathways ensures cell
72 wall integrity during normal growth as well as hostile conditions. The final, lipid-linked
73 peptidoglycan precursor lipid II is synthesized in the inner leaflet of the plasma
74 membrane by MurG, then flipped to the outer leaflet by MurJ (6) and inserted into the
75 existing cell wall by the action of transglycosylases and transpeptidases. In one
76 pathway, two dedicated enzymes work as a cognate pair, SEDS-family transglycosylase
77 RodA (7, 8), and a monofunctional, class B penicillin-binding protein (bPBP)
78 transpeptidase (9, 10). Along with cytoskeletal protein MreB, these proteins make up
79 the Rod complex. This essential pathway contributes to elongation and rod-shape
80 homeostasis by directed motion around the cell (10-13). A second, non-essential,
81 pathway utilizes bifunctional, class A PBP (aPBPs) that perform both transglycosylation
82 and transpeptidation (9, 14, 15), move diffusively, and are thought to maintain and
83 repair the cell wall (16-21). Despite a growing body of evidence suggesting that aPBPs
84 are important for stress response while the Rod complex contributes to normal growth,
85 there are also reports that Rod complex components can sense and respond to stress
86 (22-24).

87

88 While RodA and its cognate bPBP are more conserved than the aPBPs (25-27), they
89 are not found in all bacterial species (28). Even when they are encoded in the genome,

90 RodA and its bPBP are not always essential for viability nor are they always associated
91 with MreB. For example, mycobacteria and related organisms lack MreB and do not rely
92 on RodA for *in vitro* growth (29-33). Individual aPBPs are also largely dispensable for *in*
93 *vitro* growth in this genus, with *Mycobacterium smegmatis* PonA1 a notable exception
94 (9, 14, 15, 34). Why have these organisms retained enzymatically-redundant systems
95 for peptidoglycan synthesis? One clue may arise from work with the human pathogen
96 *M. tuberculosis*, where RodA and the aPBPs individually contribute to survival in
97 immune cells, some mouse backgrounds, and in a guinea pig model (29, 35-39). These
98 observations suggest that RodA and the aPBPs play unique roles in protecting
99 mycobacteria from stress.

100

101 Another way that the mycobacterial cell wall differs from those of model organisms is its
102 polar mode of elongation. Cell wall damage from external sources poses a spatial
103 challenge to pole-growing bacteria, as it presumably is not confined to the normal sites
104 of active peptidoglycan metabolism. We previously found that treatment with
105 peptidoglycan-digesting enzymes lysozyme and mutanolysin causes nascent cell wall in
106 *M. smegmatis* to shift from the poles to the sidewall (40). Here we show that *M.*
107 *smegmatis* RodA and PonA1 largely overlap in localization and activity. Upon cell wall
108 damage, peptidoglycan synthesis is redistributed from the pole to the sidewall. Neither
109 RodA nor PonA1 relocalize in a manner that corresponds to this shift; instead, the
110 redistribution of nascent cell wall correlates with that of peptidoglycan precursor
111 synthase MurG. Although not essential for growth under normal laboratory conditions,
112 RodA has a non-redundant role in damage-induced relocalization of cell wall synthesis

113 and protects *M. smegmatis* from lysis under this condition. Our data support a model in
114 which the location of precursor synthesis and use of specific transglycosylases can be
115 tuned for growth or repair.

116

117 **Results**

118 **Substantial overlap in PonA1 and RodA localization under basal conditions.** In
119 other organisms, aPBPs are hypothesized to contribute to cell wall integrity and the Rod
120 complex, to cell wall elongation (9, 10, 16, 17, 22, 41, 42). If this division of labor is true
121 in pole-growing mycobacteria, we hypothesized that RodA may be more polar than
122 aPBPs like PonA1. To test this hypothesis we sought to compare the subcellular
123 localization of fluorescent protein fusions to PonA1 and RodA. We previously confirmed
124 the functionality of an mRFP fusion to PonA1, an essential protein in *M. smegmatis*, by
125 allele swapping (43). Here we used the reduced cell length phenotype associated with
126 *rodA* deletion (29) to test and confirm functionality of our RodA-mRFP construct (Fig.
127 S1). We also showed that the fusion protein is membrane-bound, as expected, and
128 primarily detected as full-length (Fig. S2).

129 Under basal conditions, we found that RodA-mRFP and, as we and others previously
130 reported, PonA1-mRFP, are distributed along the perimeter of the mycobacterial cell
131 (43, 44) (Figs. 1a, 1b). Neither enzyme showed clear polar enrichment but RodA-mRFP
132 localization extended further towards the poles than PonA1-mRFP (Figs. 1b, 1c). mRFP
133 fusions to extracellular synthetic enzymes for other layers of the mycobacterial cell
134 envelope, including the arabinogalactan phosphotransferase Lcp1 (45), and two
135 mycolyltransferases, *MSMEG_3580* and *MSMEG_6396* (46), showed very different

136 patterns of localization from the peptidoglycan synthetic enzymes, indicating that the
137 subcellular localization patterns of RodA-mRFP and PonA1-mRFP are specific (Figs.
138 1a, 1b). These data suggest that the cell-wide distributions of the proteins largely
139 overlap, with RodA-mRFP slightly more polar than PonA1-mRFP.

140

141 **aPBPs and RodA both promote polar cell wall synthesis.** Using a variety of metabolic
142 labeling probes, we and others have found that active cell wall metabolism in
143 mycobacteria occurs in asymmetric polar gradients (40, 44, 47-52). To test whether the
144 modest difference in PonA1-mRFP and RodA-mRFP localization (Fig. 1) reflected their
145 sites of activity, we labeled nascent cell wall using the dipeptide probe alkyne-D-alanine-
146 D-alanine (53, 54). We previously showed that this probe incorporates into lipid-linked
147 peptidoglycan precursors in *M. smegmatis* and therefore is a readout for cell wall
148 biosynthesis in this species (40). To visualize aPBP activity we labeled a *rodA* knockout
149 mutant. To enrich for RodA activity, we reduced aPBP activity by moenomycin, which
150 specifically inhibits transglycosylation by aPBPs but not by RodA (8, 55-58).

151

152 The overall amount of cell wall labeling from $\Delta rodA$ or moenomycin-treated wildtype
153 cells was reduced compared to untreated wildtype (Figs. 2a,b,d). In the absence of
154 RodA, labeling was reduced along the sidewall and, to an even greater extent, at the
155 poles, such that there was a net decrease in the polarity of cell wall synthesis (Fig. 2c).
156 We observed a similar phenotype when alkyne-D-alanine-D-alanine was detected by
157 click chemistry ligation to a different fluorophore (Fig. S3). Inhibition of
158 transglycosylation by aPBPs also resulted in a labeling decrease along the sidewall

159 and, to a greater extent, at the poles (Fig. 2e). These data suggest that, under basal
160 conditions, RodA and aPBPs both contribute to polar cell wall synthesis.

161

162 **Mutanolysin/lysozyme-mediated cell wall damage occurs along the cell periphery.**

163 We previously showed that when *M. smegmatis* cells are treated with a combination of
164 lysozyme and mutanolysin, nascent peptidoglycan redistributes from the poles to the
165 sidewall (40). These enzymes are glycoside hydrolases and break the linkages that
166 connect neighbouring glycans *N*-acetylglucosamine and *N*-acetylmuramic acid in the
167 peptidoglycan backbone (Fig. S4) (3-5). We hypothesized that cell wall assembly can
168 shift to places where the cell wall is damaged, presumably for repair. Implicit in this
169 hypothesis is the assumption that enzymes added to the bacterial growth medium
170 attack the cell wall indiscriminately, *i.e.* without preference for poles vs. sidewall. In
171 support, a previous scanning electron microscopy study showed that lysozyme-
172 associated surface irregularities occur along the entire *M. smegmatis* cell periphery
173 (59). We also observed that wildtype *M. smegmatis* treated with lysozyme and
174 mutanolysin often has bumps around the cell, which we interpret as areas of weakened
175 peptidoglycan (Fig. S4), and that loss of fluorescently-labeled cell wall occurs along the
176 sidewall (Fig. S4).

177

178 **MurG relocates to the sidewall in response to cell wall damage but PonA1, RodA**

179 **and DivIVA do not.** We next considered what element(s) of cell wall assembly

180 machinery might be responsible for redistributing peptidoglycan synthesis from sites of

181 polar growth to sites of sidewall damage. After treatment with mutanolysin/lysozyme, we

182 initially found that the localization of RodA-mRFP, and to a lesser extent, PonA1-mRFP,
183 became more polar (Fig. S5). This was unexpected since nascent cell wall localization
184 shifted in the opposite direction, *i.e.* became less polar (40) (Fig. 4a). However when we
185 stained enzyme-treated cells with SYTOX Green, a dye that preferentially labels dead
186 bacteria, we did not observe any viable cells with relocalized RodA-mRFP (Fig. S6).
187 While we do not yet understand this phenotype, quantification of RodA-mRFP
188 fluorescence from SYTOX Green-excluded cells suggests that cell wall damage likely
189 does not change the localization of extracellular synthesis proteins (Fig. S6).

190

191 In contrast to well-studied, rod-shaped species, mycobacteria coordinate cell wall
192 synthesis via the cytoskeletal protein DivIVA (Wag31), rather than MreB (50, 60-62). We
193 wondered whether DivIVA might also organize cell wall synthesis in response to
194 sidewall damage. However the location of the functional fluorescent protein fusion
195 DivIVA-eGFP (40, 50, 62), like those of PonA1 and RodA, did not change upon
196 mutanolysin/lysozyme treatment (Fig. 3a).

197

198 We next turned our attention to the source of peptidoglycan precursor substrates for the
199 aPBPs and RodA. Synthesis of the final precursor lipid II is carried out by MurG.
200 Accordingly we treated cells expressing the functional fluorescent protein fusion MurG-
201 Dendra2 (43) with mutanolysin/lysozyme. Imaging of cells before and after treatment
202 revealed that MurG-Dendra2 signal transitions from a predominantly sub-polar and
203 patchy signal to a more uniform signal that often surrounds the entire periphery of the
204 cell (Fig. 3b). Because relocalization of RodA-mRFP was only observed in dead cells,

205 we stained both untreated and treated cells with propidium iodide, another dye that
206 preferentially labels dead bacteria. After omitting propidium iodide-stained cells from our
207 analysis, fluorescence quantitation supported our observation that MurG-Dendra2
208 relocalizes away from the polar region upon cell wall damage (Figs. 3c-e) and that it
209 becomes less patchy (Fig. 3f).

210

211 Taken together, our data indicate that MurG, but not PonA1, RodA or DivIVA,
212 relocalizes upon cell wall damage.

213

214 **RodA, but not aPBPs contributes to redistribution of peptidoglycan synthesis**

215 **upon cell wall damage.** The distribution of MurG, and therefore lipid II, likely
216 contributes to spatial flexibility in peptidoglycan assembly. The location of RodA (and
217 likely, PonA1) did not obviously change upon cell wall damage (Fig. S5, S6). However,
218 given the basal, cell-wide distribution of both transglycosylases, we asked if they might
219 contribute to damage-induced pole-to-sidewall redistribution of nascent peptidoglycan.

220 We first reproduced the cell wall labeling phenotype in mutanolysin/lysozyme-treated
221 wildtype *M. smegmatis* (40) and showed that there was a decrease in nascent

222 peptidoglycan polarity (Fig. 4a). By contrast, we found that mutanolysin/lysozyme

223 treatment of *M. smegmatis* lacking RodA did not change the polarity of nascent

224 peptidoglycan (Fig. 4b, Fig. S3). However, pretreating wildtype cells with the aPBP-

225 transglycosylation inhibitor moenomycin did not prevent pole-to-sidewall damage

226 response (Fig. 4c). These data suggest that RodA, but not aPBPs, contributes to stress-

227 induced spatial flexibility in peptidoglycan synthesis.

228

229 **A non-redundant role for RodA in protection against cell wall damage.** The
230 contribution of RodA_{Mtb} to *M. tuberculosis* survival in different *in vivo* models (29, 35-37,
231 39) and the requirement for RodA_{Msm} in the damage-induced sidewall shift in *M.*
232 *smegmatis* peptidoglycan synthesis (Fig. 4) suggested that the enzyme could play a
233 non-redundant role in protecting against cell wall stress. To test, we challenged wild-
234 type and $\Delta rodA$ *M. smegmatis* cultures in the presence or absence of moenomycin with
235 mutanolysin/lysozyme and plated spot dilutions (Fig. S7). For reasons that we do not
236 yet understand, moenomycin treatment appeared to reduce the sensitivity of *M.*
237 *smegmatis* to cell wall damage. Because the spot dilutions did not have the resolution to
238 test whether there was a difference between wildtype and $\Delta rodA$, we performed full-
239 plate colony-forming unit (CFU) assays and microscopy at several time points. Upon
240 addition of mutanolysin/lysozyme to the growth medium, wildtype *M. smegmatis* grew
241 for 2 hours prior to lysing (Fig. 5a) albeit more slowly than untreated cells (Fig. 5b). By
242 contrast $\Delta rodA$ immediately began to lyse, a phenotype evident both by CFUs and by
243 microscopy (Fig. 5a, Fig. S4). $\Delta rodA$ lysis was complemented by expression of *rodA*-
244 mRFP (Fig. 5b). Expression of *rodA*-mRFP in a wildtype background, moreover,
245 enhanced survival compared to wildtype alone (Fig. 5b). Thus while RodA is
246 dispensable for normal growth (29) (Fig. S8), it plays a non-redundant role in protection
247 from cell wall damage.

248

249

250

251 **Discussion**

252

253 We have previously shown that upon cell wall insult, peptidoglycan assembly in *M.*
254 *smegmatis* relocates from the growing poles to the non-growing sidewall (40). Given
255 that bacteria are likely to encounter such insults frequently in their natural habitats, we
256 sought to better understand the factors that drive relocalization. We focused on the
257 roles of two peptidoglycan transglycosylases, the aPBP PonA1 and SEDS family
258 transglycosylase RodA.

259

260 In laterally-growing, rod-shaped bacteria, the emerging narrative is that RodA lays the
261 template for elongation and aPBPs fill in the gaps for maintenance and repair (10, 16-
262 19, 21). Unlike the organisms in which this model has been tested, pole-growing
263 bacteria like members of the Mycobacteriales and Hyphomicrobiales lack the
264 cytoskeletal protein MreB and either lack or do not require RodA for viability or shape
265 (28, 29). If the division of labor that has been reported in laterally-growing bacilli were
266 employed by mycobacteria, we would predict that localization and activity of RodA
267 would be enriched at the poles, while localization and activity of aPBPs like PonA1
268 would be distributed around the cell periphery. This is reminiscent of the model for
269 transpeptidation in mycobacterial peptidoglycan, where the D,D-transpeptidases that
270 catalyze 4,3-crosslinks associated with lipid II insertion are likely to be enriched at the
271 poles and the L,D-transpeptidases that catalyze 3,3-crosslinks associated with cell wall
272 maturation localize along the cell periphery (40, 44, 63, 64). Instead we observed that
273 the distributions of functional fluorescent protein fusions to RodA and PonA1 are similar,

274 as are their enzymatic activities (Figs. 1-2). As recent findings in pole-growing
275 *Corynebacterium glutamicum* (31) also suggest, the division of labor for *M. smegmatis*
276 peptidoglycan polymerases under basal conditions is subtle.

277 While RodA and aPBPs make similar contributions to polar growth, our data suggest
278 that their roles diverge upon cell wall damage (Fig. 5). Specifically, RodA plays a non-
279 redundant role in damage-associated pole-to-sidewall redistribution of peptidoglycan
280 synthesis, which is concomitant with a similar redistribution of the lipid II synthase MurG
281 (Fig. 3). It is not yet clear if the change in substrate availability is the cause,
282 consequence or simply occurs in parallel with the change in transglycosylase usage. In
283 the future, localization of lipid II flippase MurJ—which bridges lipid II synthesis in the
284 inner leaflet and lipid II insertion in the outer leaflet—may help us to distinguish between
285 these models. In *Staphylococcus aureus*, MurJ recruitment redirects peptidoglycan
286 synthesis from the cell periphery, for expansion, to midcell, for division (65).

287 Our data suggest that RodA promotes a pole-to-sidewall shift in peptidoglycan synthesis
288 (Fig. 4) and survival during cell wall damage (Fig. 5). The non-redundant role(s) for
289 RodA in resistance to lysis (Fig. 5) is consistent with at least two models. In the first,
290 RodA provides on-demand repair of cell wall damage. A similar stress-specific,
291 peptidoglycan-building role for RodA has been suggested in *Listeria monocytogenes*
292 (24), where absence of a RodA homolog also sensitizes bacteria to cell wall damage
293 (66). Loss of damage-induced sidewall shift supports this type of active role for RodA in
294 mycobacteria. However if true, this would be in contrast to the repair function of aPBPs,
295 rather than RodA, in other organisms (16-19, 21). Thus a second model to explain the

296 lysis phenotype of $\Delta rodA$ is that RodA builds a cell wall with an architecture that is
297 inherently more resistant to damage or that is more amenable to repair.

298

299 The utility of two pathways for the same enzymatic reaction is not clear under
300 laboratory-optimized growth conditions. By studying the requirements for peptidoglycan
301 synthesis during cell wall damage, we have uncovered spatial flexibility in precursor
302 synthesis and extracellular insertion, and a non-redundant role for RodA in protection
303 (Fig. 6). These factors may enable mycobacteria to balance polar growth with cell-wide
304 repair in the host and soil environments.

305 **Materials and Methods**

306 **Strain construction.** Genes of interest were amplified from *M. smegmatis*
307 mc²155 genomic DNA. *mRFP* was amplified from a pL5pTetO plasmid, with primers in
308 Table S1. Backbone plasmid pL5pTetO was linearized by PCR. 15 ng of plasmid
309 backbone, 20 ng of gene of interest, and 20 ng of *mRFP* PCR products were incubated
310 with Gibson master mix (New England Biolabs, #E2611S) at 50°C for 1 hour. 5 μ L of
311 Gibson product was transformed into 50 μ L XL1-Blue *E. coli* competent cells by heat
312 shock. Transformants on 50 μ g/mL kanamycin plates were confirmed by colony PCR
313 and sequencing, and then electroporated into *M. smegmatis* mc²155 or into $\Delta rodA$.

314

315 **Cell wall damage.** Wildtype or $\Delta rodA$ cells were grown to stationary phase, then back-
316 diluted and allowed overnight growth to log phase (OD₆₀₀ = 0.5-0.8). Lysozyme (Sigma-
317 Aldrich, #L6876) was freshly resuspended in PBS, filter-sterilized, and added to cultures

318 at a final concentration of 500 µg/mL. Mutanolysin (Sigma-Aldrich #M9901) was added
319 simultaneously at a final concentration of 500 U/mL. Cultures were incubated at 37°C
320 shaking at 300 rpm for 1 hour.

321 **Peptidoglycan labeling.** Peptidoglycan precursor probe alkyne-D-alanine-D-alanine (2
322 mM; custom synthesized by WuXi AppTech), was added to cultures for the final
323 10 minutes of incubation. Cells were washed three times in cold PBS and fixed in 2%
324 formaldehyde for 10 minutes. Cells were washed in PBS then subjected to CuAAC with
325 picolyl azide-AF488 or picolyl azide-TAMRA (Click Chemistry Tools) as described (67,
326 68).

327

328 **CFUs and growth curves.** Wildtype + pL5pTetO, wildtype + pL5pTetO-*rodA-mRFP*,
329 Δ rodA + pL5pTetO, and Δ rodA + pL5pTetO-*rodA-mRFP* cells were grown to stationary
330 phase, then back-diluted and allowed to grow overnight to log phase ($OD_{600} = 0.5-0.8$).
331 Cultures were back-diluted once more to $OD_{600} = 0.05$. Lysozyme and mutanolysin were
332 added as above. Triplicate cultures were incubated at 37°C shaking at 150 rpm for 5
333 hours. Aliquots were periodically plated for CFUs.

334

335 **Moenomycin treatment.** Wildtype cells were grown to stationary phase, then back-
336 diluted and allowed to grow overnight to log phase ($OD_{600} = 0.5-0.8$). Moenomycin
337 (Cayman Chemicals, #15506) was added at concentrations described in text. Cultures
338 were incubated at 37°C shaking at 400 rpm for 30 minutes in Benchmark Scientific
339 MultiTherm Shaker H5000-H.

340

341 **Viability staining.** Staining was calibrated using untreated cells as live control and 70%
342 isopropanol-treated cells as dead control. Following 90 minute treatment with lysozyme
343 and mutanolysin, cells expressing RodA-mRFP were washed with HEPES-buffered
344 saline (HBS) twice, and resuspended in HBS + Sytox Green (Fisher Scientific, #S7020)
345 at a final concentration of 2.5 μ M. For cells expressing MurG-Dendra2, propidium iodide
346 was added to a final concentration of 4 μ M. Cells were then incubated in the dark for an
347 additional 30 minutes and imaged immediately.

348

349 **Imaging.** Cells were placed on pads made of 1% agarose in water. Images were
350 acquired on Nikon Eclipse E600 at exposure times detailed in main text.

351

352 **Image analysis.** Cell outlines were traced using Oufi (69). Demographs were
353 generated using tools built into the program. Intensity profiles of non-septating labeled
354 cells only were generated using MATLAB code described in (40). Polarity ratios were
355 calculated by combining signal values for 15% of the cell length on either pole and
356 dividing the sum by total cell fluorescence. Beeswarm plots and boxplots generated on
357 R studio. Super plots were generated as described in (70).

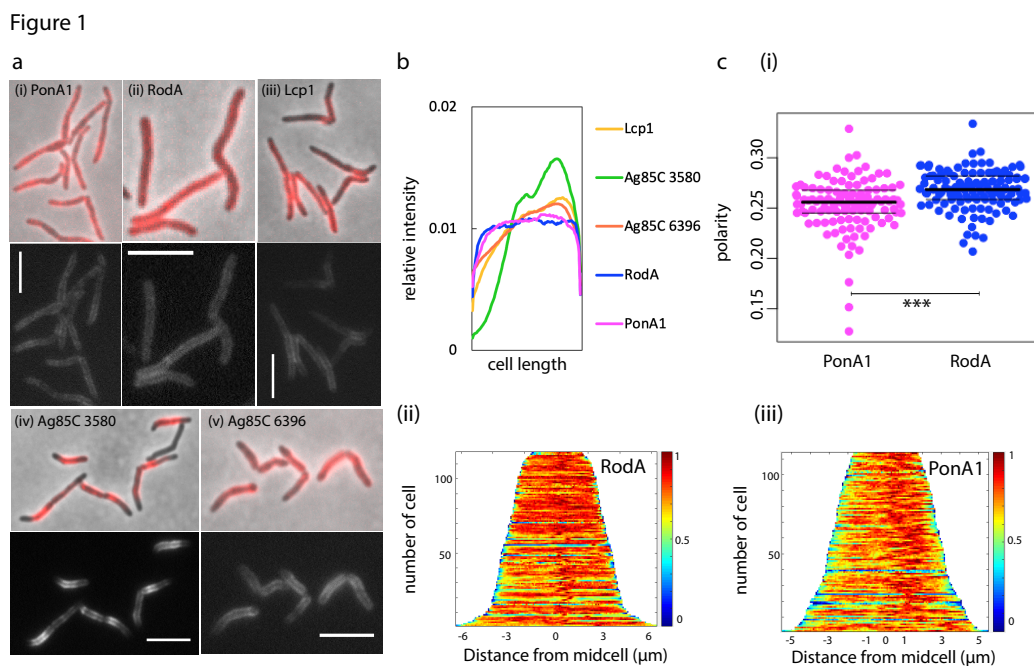
358

359 **Membrane fractionation and western blotting.** Wildtype *M. smegmatis* and cells
360 expressing RodA-mRFP were grown to OD₆₀₀ ~0.6 and lysed by nitrogen cavitation.
361 Lysates were separated into cytoplasm and membrane fractions by ultracentrifugation
362 at 35,000 rpm for 2 hours. Protein concentration was adjusted to 560 μ g/mL. Cell lysate
363 or fractionated samples were separated by SDS-PAGE on a 4-20% polyacrylamide gel

364 and transferred to a PVDF membrane. The membrane was blocked with 3% skim milk
 365 in PBS + 0.05% Tween-80 (PBST) and then incubated overnight with primary
 366 monoclonal mouse anti-RFP. Antibodies were detected with appropriate secondary
 367 antibodies conjugated to horseradish peroxidase (GE Healthcare, Chicago, IL).
 368 Membranes were rinsed in PBS + 0.05% Tween-20 before visualization.

369

370 **Main Figures**

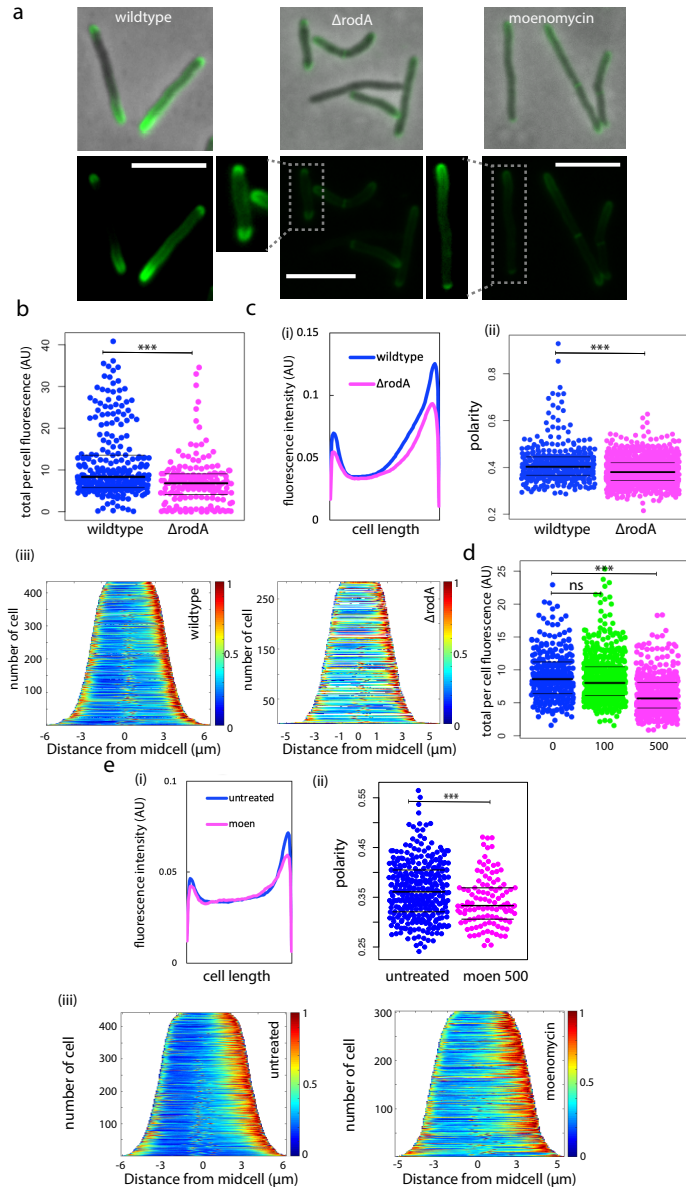


371

372 **Figure 1: RodA and PonA1 localize around cell periphery under basal conditions.**

373 (a) Enzymes involved in (i, ii) peptidoglycan-, (iii) arabinogalactan-, and (iv, v)
 374 mycomembrane synthesis were fused to mRFP and imaged at exposure of (i) 5 s or (ii-
 375 v) 4 s. Scale bars = 5 μm . (b) Normalized fluorescence intensity profiles for mRFP
 376 tagged enzymes. $93 < n < 121$. (c) Localization of RodA-mRFP and PonA1 compared by
 377 (i) polarity ratio calculated as the signal from 15% of the cell length on either pole,

378 divided by signal from the entire cell. *t*-test, $p < 0.001$; (ii,iii) normalized demographs.
379 112<n<118.



380

381 **Figure 2: RodA and aPBPs promote polar peptidoglycan synthesis under basal**

382 **conditions.** (a) wildtype *M. smegmatis*, $\Delta rodA$, and *M. smegmatis* treated with

383 moenomycin for 30 minutes were incubated with alkyne-D-alanine-D-alanine for 10

384 minutes (~5-6% generation time). Probe was detected by click chemistry ligation to

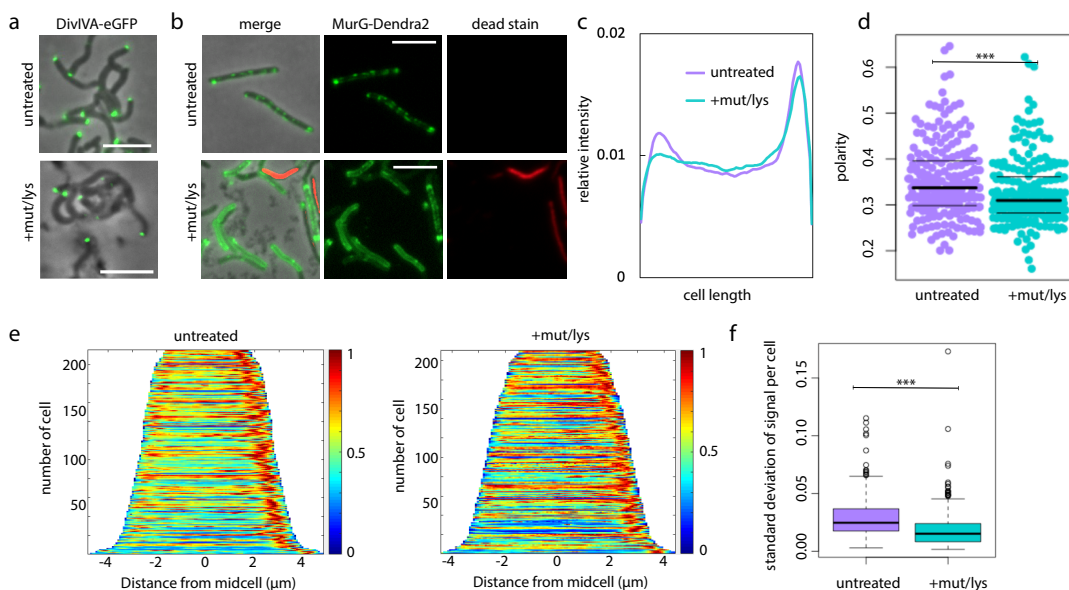
385 picolyl azide AF488. All images acquired at 1 s exposure. Dim signal from boxed cells
386 enhanced for visibility. Scale bars = 5 μm (b) Total fluorescence per cell. *t*-test, $p <$
387 0.001 (c) Fluorescence signal localization of wildtype *M. smegmatis* and ΔrodA
388 represented by (i) raw fluorescence intensity profile; (ii) polarity ratio. *t*-test, $p < 0.001$
389 (iii) demographs. $168 < n < 816$. Representative of three independent experiments (d)
390 Total fluorescence per cell following 30 minutes of 0, 100, or 500 $\mu\text{g}/\text{mL}$ moenomycin.
391 Significance determined using analysis of variance (ANOVA) followed by a Tukey post
392 hoc test to conduct pairwise comparisons. ***, $p < 0.001$ (e) Fluorescence signal
393 localization from wildtype cells untreated and treated with 100 or 500 $\mu\text{g}/\text{mL}$
394 moenomycin for 30 minutes represented by (i) raw fluorescence intensity profile; (ii)
395 polarity ratio, *t*-test, ***, $p < 0.005$; (iii) demographs. $285 < n < 433$.

396

397

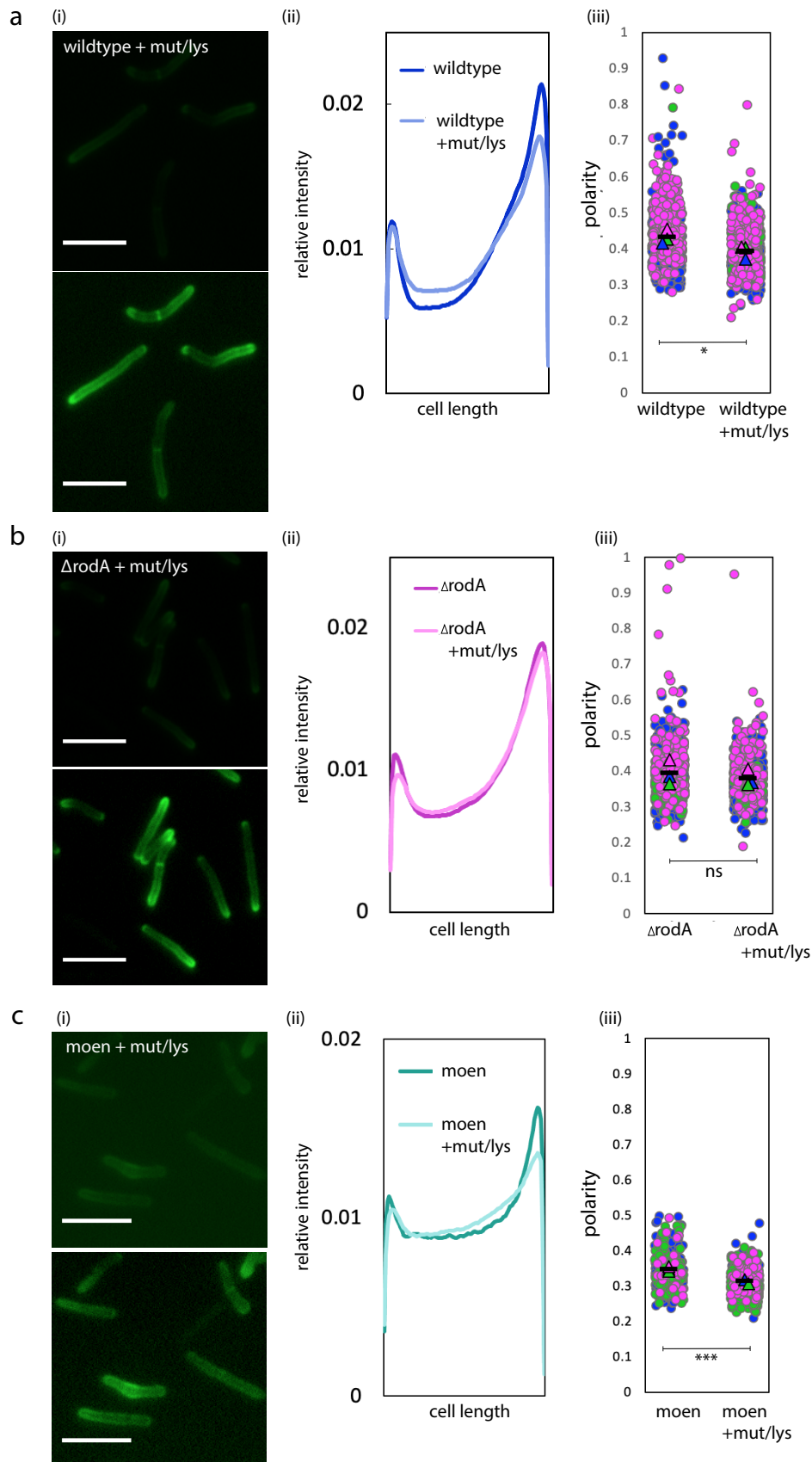
398

399

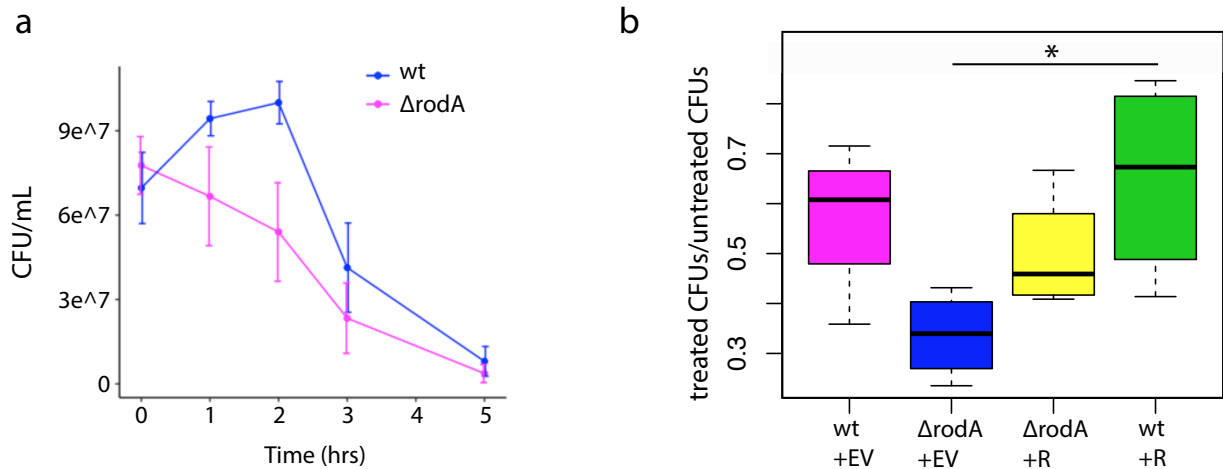


400

401 **Figure 3: MurG relocates upon cell wall damage.** (a) Cells expressing the DivIVA-
402 eGFP (50) were treated +/- mutanolysin/lysozyme. Scale bars = 5 μm (b) Cells
403 expressing the functional fusion MurG-Dendra2 (43) were treated +/-
404 mutanolysin/lysozyme, then stained with propidium iodide for detection of dead cells. 3
405 s exposure for green channel, 500 ms exposure for red channel. Scale bars = 5 μm. (c)
406 Normalized MurG-Dendra2 fluorescence intensity profiles (d) Polarity ratio of MurG-
407 Dendra2 signal. *t*-test, $p < 0.001$. (e) MurG-Dendra2 demographs. (f) Standard deviation
408 calculated for 100 fluorescence values per cell in untreated and treated cells. *t*-test, $p <$
409 0.001. $210 < n < 215$.

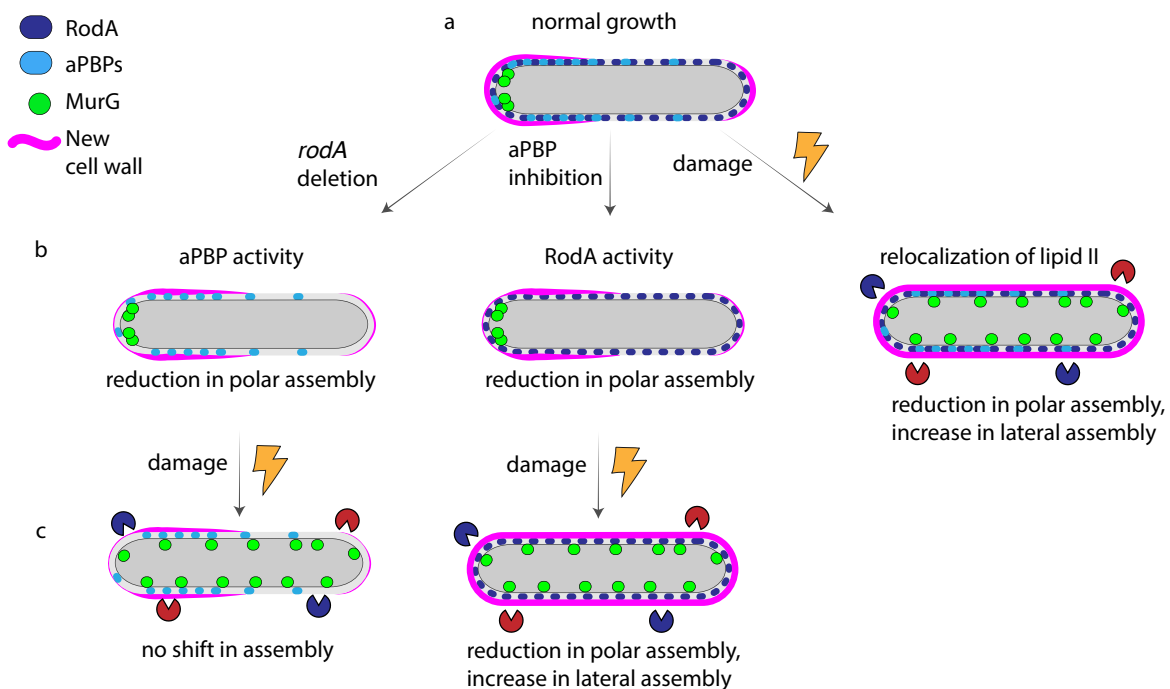


411 **Figure 4: RodA contributes to damage-induced relocalization of peptidoglycan**
412 **assembly.** At the end of lysozyme/mutanolysin treatment, nascent cell wall in wild-type
413 (a) or $\Delta rodA$ (b) or moenomycin treated cells (c) was labeled with alkyne-D-alanine-D-
414 alanine as in Fig. 2a and (i) imaged at 1s exposure (bottom panel is the same image
415 with enhanced signal for visualization), compare to untreated in Fig. 2a (ii) Normalized
416 fluorescence intensity profiles comparing relative signal from untreated and treated
417 cells. (iii) Super plots of cell wall labeling polarity ratio (signal from both poles divided by
418 total cell fluorescence) from 3 independent experiments, each color represents an
419 experiment. *t*-test in (a), $p < 0.05$, (b), $p > 0.1$, (c), $p < 0.01$ $102 < n < 826$. Scale bars = 5
420 μm .
421



422
423 **Figure 5: RodA protects against cell wall damage.** (a) Colony forming units (CFU)
424 over time for wildtype and $\Delta rodA$ cells +/- mutanolysin/lysozyme. $n = 3$. Compare to
425 Figure S8 (b) Ratios of treated/untreated CFUs after 2 hours of mutanolysin/lysozyme,
426 comparing wildtype + empty vector (EV), $\Delta rodA$ + empty vector, $\Delta rodA$ + *rodA-mRFP*

427 (R), wildtype + *rodA-mRFP*. While cultures were normalized to $OD_{600} = 0.05$ prior to
 428 treatment, the uncomplemented mutant and RodA overexpression strains consistently
 429 had higher and lower CFU than wildtype at $t = 0$, respectively. This is likely due to the
 430 differences in cell length between the four strains (29) (Fig. S1). To better highlight the
 431 effects of mutanolysin/lysozyme we calculated the fold change in CFU between treated
 432 and untreated cells after two hours. $n = 4$ independent experiments, two of which done
 433 in triplicate. Significance determined using analysis of variance (ANOVA) followed by a
 434 Tukey post hoc test to conduct pairwise comparisons. *, $p < 0.05$, only significant
 435 relationship portrayed.
 436
 437



439 **Figure 6: Spatial flexibility model for peptidoglycan assembly.** (a) under basal
 440 conditions PonA1 and RodA overlap substantially but not completely; new cell wall is

441 assembled asymmetrically and enriched at the poles. (b, left and middle) upon *rodA*
442 deletion and aPBP inhibition new cell wall assembly is disproportionately reduced at the
443 poles. (b, right) upon cell wall damage MurG redistributes from the poles to the cell
444 periphery, as does new cell wall. (c, left) in the absence of RodA cell wall assembly is
445 not shifted to the lateral cell under stress. (c, right) when aPBPs are inhibited cell wall
446 assembly redistributes upon damage.

447

448

449

450

451

452

453

454

455

456

457

458

459

460

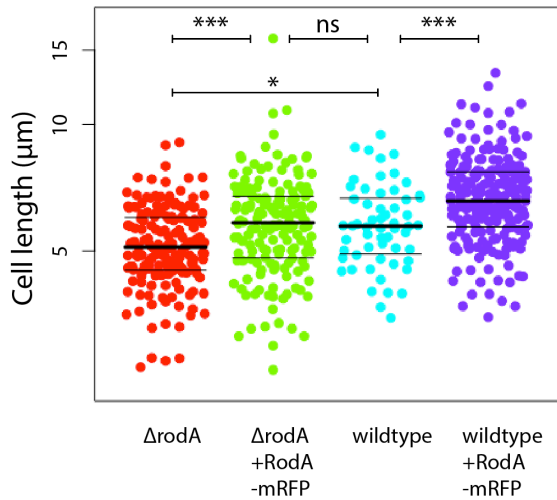
461

462

463

464 **Supplementary data**

465



466

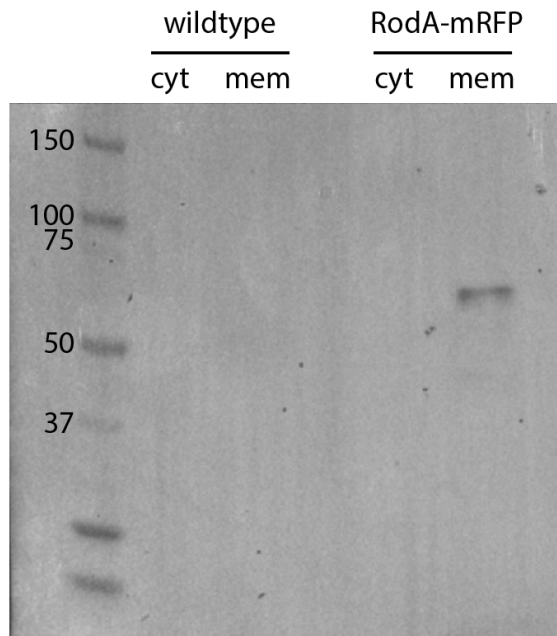
467 **Figure S1: RodA-mRFP fusion complements ΔrodA .** Phase images of ΔrodA +
468 empty vector, ΔrodA + *rodA-mRFP*, wildtype + empty vector, and wildtype + *rodA-mRFP*
469 were acquired and cell lengths were quantified using Oufiti (69), MATLAB, and
470 visualized using R Studio (58<n<204). Significance determined using analysis of
471 variance (ANOVA) followed by a Tukey post hoc test to conduct pairwise comparisons.
472 ns, not significant; *, $p<0.05$; **, $p<0.01$; ***, $p<0.005$.

473

474

475

476



477

478 **Figure S2: RodA-mRFP fusion localizes to the plasma membrane with**

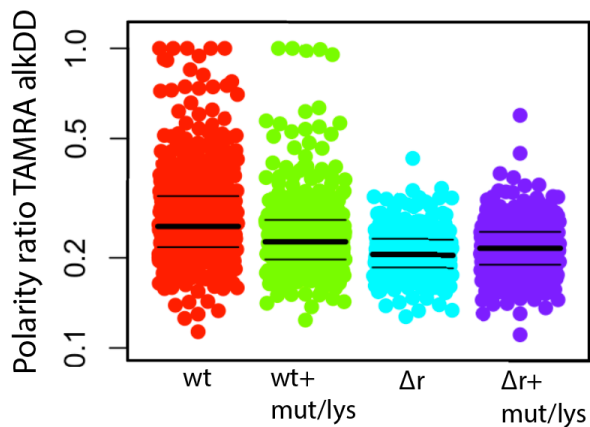
479 **minimal degradation.** Lysates from *M. smegmatis* +/- *rodA-mRFP* were

480 separated into cytoplasmic (cyt) and membrane (mem) fractions by

481 ultracentrifugation and immunoblotted with anti-RFP antibodies. Protein

482 concentration normalized.

483

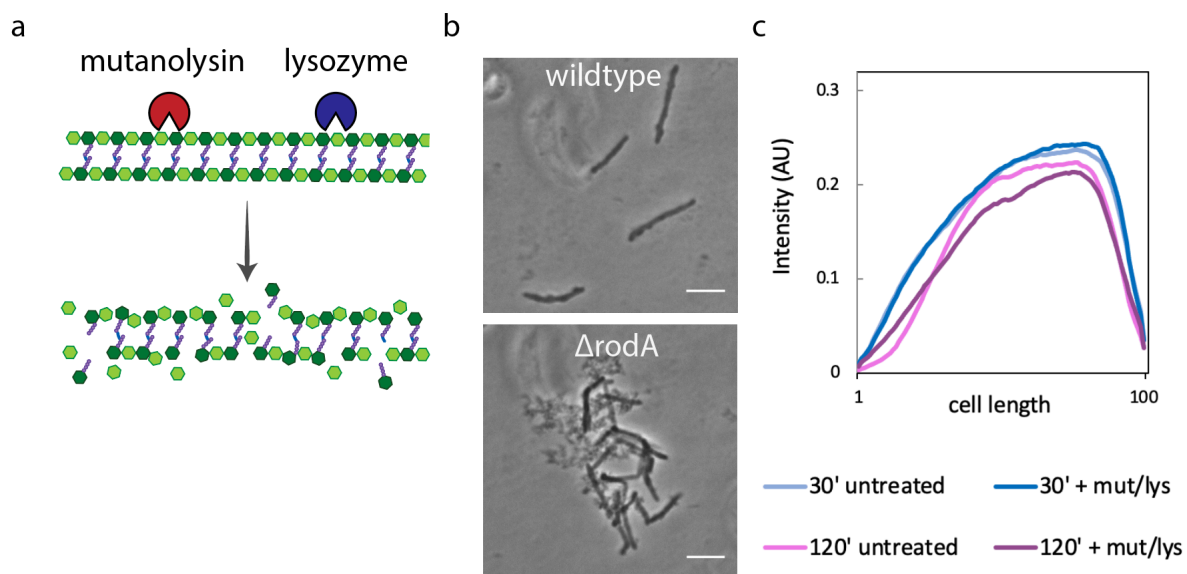


484

485 **Figure S3: Polarity of cell wall synthesis detected with TAMRA.** Polarity ratio of cell
486 wall labeling (bright pole signal/total cell fluorescence) in wildtype and $\Delta rodA$ +/-
487 mutanolysin/lysozyme. Nascent peptidoglycan labeled as in Fig. 2a except that click
488 chemistry detection was with picolyl azide-TAMRA.

489

490



491

492 **Figure S4: Mutanolysin/lysozyme treatment leads to cell-wide damage.** (a)

493 Muramidases mutanolysin and lysozyme break the linkages between neighbouring
494 glycans *N*-acetylglucosamine and *N*-acetylmuramic acid in the peptidoglycan backbone

495 (b) Phase contrast images of wildtype or $\Delta rodA$ *M. smegmatis* +/-

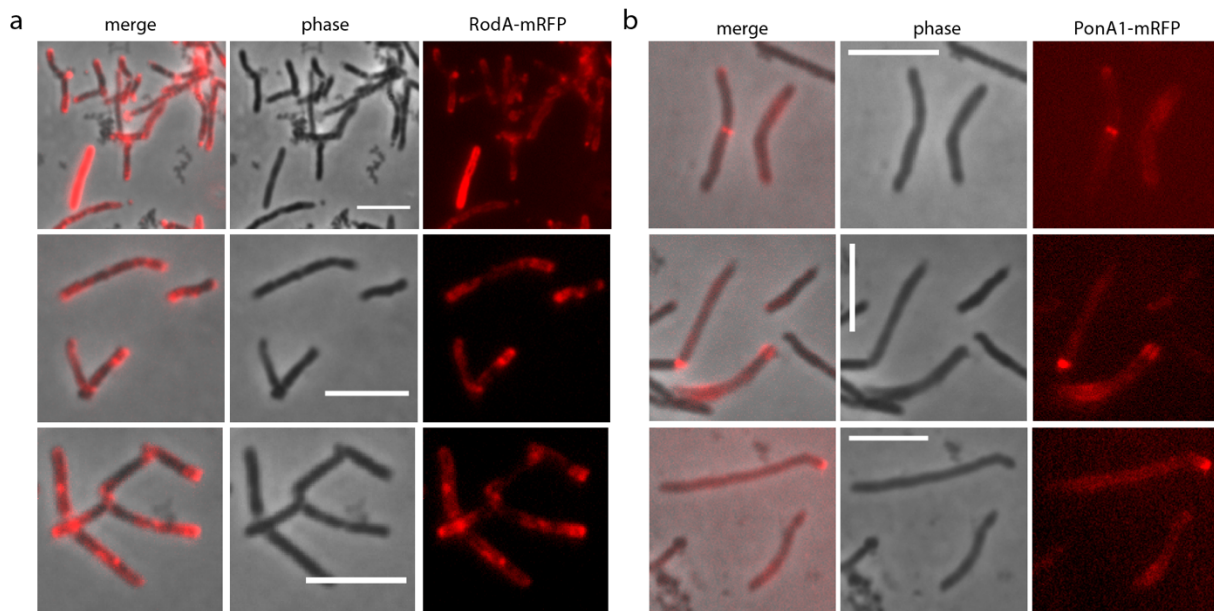
496 mutanolysin/lysozyme. Scale bars = 5 μ m. (c) *M. smegmatis* was labeled with 1 μ M

497 RADA, a D-amino acid mono-peptide that we previously showed incorporates into

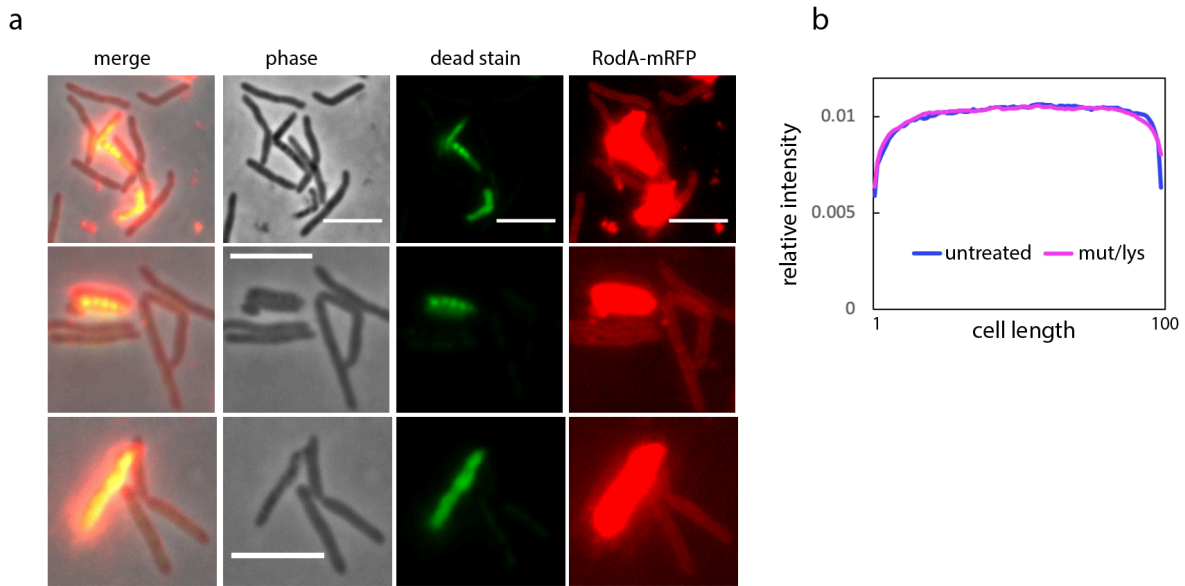
498 peptidoglycan via L,D-transpeptidases (40) and coats the cell wall evenly after overnight

499 incubation with a low concentration (62). After washing, the culture was treated with

500 mutanolysin/lysozyme and loss of fluorescence along the length of the cells was
501 quantitated. As expected, after 2 hours labeling loss was observed at the poles in
502 untreated cells. Loss of fluorescence at the poles of lysozyme/mutanolysin-treated *M.*
503 *smegmatis* was not as pronounced, consistent with its slow growth in the presence of
504 the enzymes (Figure 5a). At this time point, sidewall loss of fluorescence was greatly
505 enhanced with enzyme treatment. Although mycobacterial growth precludes
506 interpretation of cell wall loss at the poles, these data suggest that
507 lysozyme/mutanolysin-mediated cell wall loss occurs along the *M. smegmatis* sidewall.
508 Signal not normalized. 58<n<102.



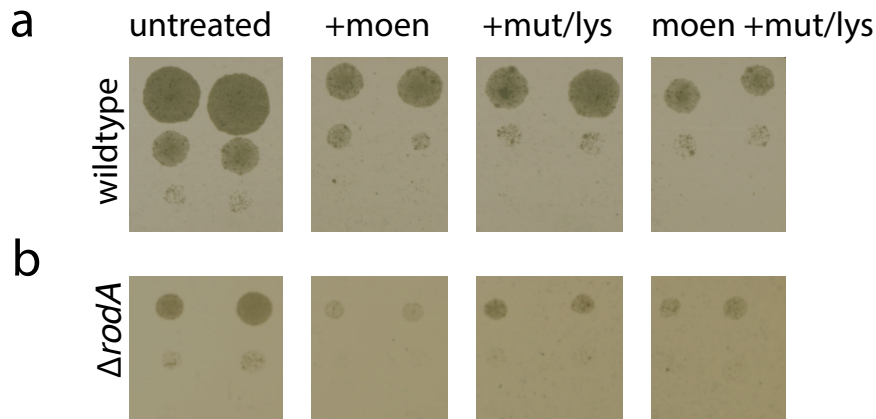
509
510 **Figure S5: RodA-mRFP and PonA1-mRFP location in cells treated with**
511 **lysozyme/mutanolysin.** Representative images of (a) RodA-mRFP and (b) PonA1-
512 mRFP imaged following mutanolysin/lysozyme treatment. Compare to Figure 1a. Scale
513 bars = 5 μm .



514

515 **Figure S6: RodA relocation is not observed in live cells.** (a) Staining with dead
516 stain SYTOX green reveals that there are no viable cells that display RodA-mRFP polar
517 relocation phenotype associated with mutanolysin/lysozyme treatment. Scale bars =
518 5 μm . (b) Cells expressing RodA-mRFP were treated +/- mutanolysin/lysozyme then
519 stained with SYTOX green. Only cells that did not stain green, *i.e.*, deemed viable, were
520 included in Oufiti followed by MATLAB analysis.

521



522

523 **Figure S7: Effect of moenomycin and cell wall digesting enzymes on growth of**

524 **wildtype and $\Delta rodA$.** (a) Wildtype and (b) $\Delta rodA$ *M. smegmatis* were treated +/-

525 moenomycin (moen) for 30 minutes; mutanolysin/lysozyme (mut/lys) for 60 minutes; or

526 moenomycin followed by mutanolysin/lysozyme. Tenfold serial dilutions were plated

527 following indicated treatment. Moenomycin inhibits growth of wildtype and of $\Delta rodA$ *M.*

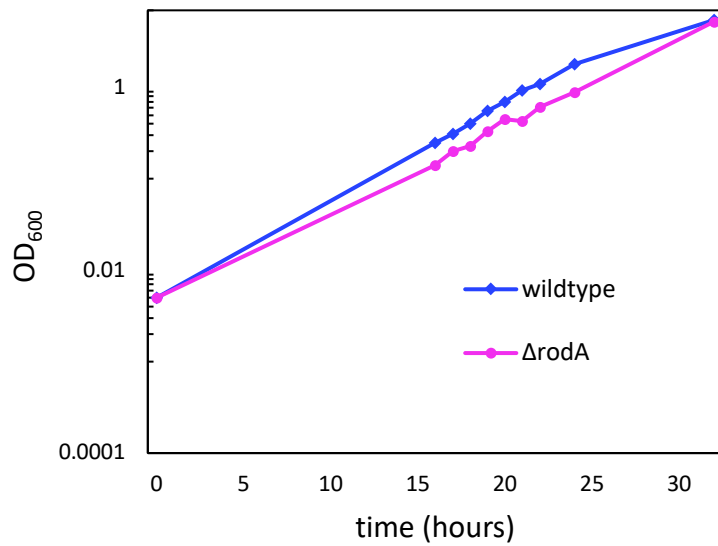
528 *smegmatis*; Mutanolysin/lysozyme treatment also inhibits growth in both strains;

529 Combination of moenomycin and mutanolysin/lysozyme treatments does not have an

530 obvious additive effect in either strain. Experiment was performed in triplicate and

531 representative data are shown. a and b not comparable.

532



533

534 **Figure S8: RodA is not required for growth in *M. smegmatis*.**

535

536

537

538 **Table S1: Primers used for fluorescent fusion constructs.**

539

gene of interest	primers for <i>M. smegmatis</i> gene
<i>rodA-mRFP</i>	TTAATTAAGAAGGAGATATACATatgatgacgacgcaaccccag
	gaCGTCCTCGGAGGAGGCcgagccgcctaccttttcgatcacctcgg
<i>lcp1-mRFP</i>	GCTTAATTAAGAAGGAGATATACATatggtgatcagggtccattgctgtg
	CGTCCTCGGAGGAGGCcgagccgccgttcacgcactgcgggtcggttg
	CTTAATTAAGAAGGAGATATACATatgcgcggcattgcagcatggaag

<i>fbpC</i> (MSMEG_3580))-mRFP	GTCCTCGGAGGAGGCcgagccgcccgtggcggactgagcgccgagcacc
<i>fbpC</i> (MSMEG_3580))-mRFP	CTTAATTAAGAAGGAGATATACATatgagacgtgggtgagtctggttc CGTCCTCGGAGGAGGCcgagccgcccttgatggtggcgaccagctcacc
	<i>mRFP primers</i>
<i>rodA-mRFP</i>	gatcgaaaaggtaggcggctcgGCCTCCTCCGAGGACGtcatca CCCAATTAATTAGCTAAAGCTTtcaGGCGCCGGTGGAGTGgc
<i>lcp1-mRFP</i>	gatgaCGTCCTCGGAGGAGGCcgagccgcccgttcacgcactgcgggtcg CCCAATTAATTAGCTAAAGCTTtcaGGCGCCGGTGGAGTGgcggc cctc
<i>fbpC</i> (MSMEG_3580))-mRFP	gatgaCGTCCTCGGAGGAGGCcgagccgcccgtggcggactgagcgccg CCCAATTAATTAGCTAAAGCTTtcaGGCGCCGGTGGAGTGgcggc cctc
<i>fbpC</i> (MSMEG_3580))-mRFP	gatgaCGTCCTCGGAGGAGGCcgagccgcccttgatggtggcgaccagc CCCAATTAATTAGCTAAAGCTTtcaGGCGCCGGTGGAGTGgcggc cctc

540

541

542

543

544 References

545

546

547

- 548 1. Fernandes S, Sao-Jose C. 2018. Enzymes and Mechanisms Employed by Tailed
549 Bacteriophages to Breach the Bacterial Cell Barriers. *Viruses* 10.
- 550 2. Hamada S, Torii M, Kotani S, Masuda N, Ooshima T, Yokogawa K, Kawata S. 1978.
551 Lysis of *Streptococcus mutans* cells with mutanolysin, a lytic enzyme prepared from a
552 culture liquor of *Streptomyces globisporus* 1829. *Arch Oral Biol* 23:543-9.
- 553 3. Ragland SA, Criss AK. 2017. From bacterial killing to immune modulation: Recent
554 insights into the functions of lysozyme. *PLoS Pathog* 13:e1006512.
- 555 4. Stamp GW, Poulson R, Chung LP, Keshav S, Jeffery RE, Longcroft JA, Pignatelli M,
556 Wright NA. 1992. Lysozyme gene expression in inflammatory bowel disease.
557 *Gastroenterology* 103:532-8.
- 558 5. Nash JA, Ballard TN, Weaver TE, Akinbi HT. 2006. The peptidoglycan-degrading
559 property of lysozyme is not required for bactericidal activity in vivo. *J Immunol* 177:519-
560 26.
- 561 6. Barreteau H, Kovac A, Boniface A, Sova M, Gobec S, Blanot D. 2008. Cytoplasmic
562 steps of peptidoglycan biosynthesis. *FEMS Microbiol Rev* 32:168-207.
- 563 7. Emami K, Guyet A, Kawai Y, Devi J, Wu LJ, Allenby N, Daniel RA, Errington J. 2017.
564 RodA as the missing glycosyltransferase in *Bacillus subtilis* and antibiotic discovery for
565 the peptidoglycan polymerase pathway. *Nat Microbiol* 2:16253.
- 566 8. Meeske AJ, Riley EP, Robins WP, Uehara T, Mekalanos JJ, Kahne D, Walker S, Kruse
567 AC, Bernhardt TG, Rudner DZ. 2016. SEDS proteins are a widespread family of
568 bacterial cell wall polymerases. *Nature* 537:634-638.
- 569 9. Zhao H, Patel V, Helmann JD, Dorr T. 2017. Don't let sleeping dogmas lie: new views of
570 peptidoglycan synthesis and its regulation. *Mol Microbiol* 106:847-860.
- 571 10. Cho H, Wivagg CN, Kapoor M, Barry Z, Rohs PDA, Suh H, Marto JA, Garner EC,
572 Bernhardt TG. 2016. Bacterial cell wall biogenesis is mediated by SEDS and PBP
573 polymerase families functioning semi-autonomously. *Nat Microbiol* 1:16172.
- 574 11. Dominguez-Escobar J, Chastanet A, Crevenna AH, Fromion V, Wedlich-Soldner R,
575 Carballido-Lopez R. 2011. Processive movement of MreB-associated cell wall
576 biosynthetic complexes in bacteria. *Science* 333:225-8.
- 577 12. Garner EC, Bernard R, Wang W, Zhuang X, Rudner DZ, Mitchison T. 2011. Coupled,
578 circumferential motions of the cell wall synthesis machinery and MreB filaments in *B.*
579 *subtilis*. *Science* 333:222-5.
- 580 13. van Teeffelen S, Wang S, Furchtgott L, Huang KC, Wingreen NS, Shaevitz JW, Gitai Z.
581 2011. The bacterial actin MreB rotates, and rotation depends on cell-wall assembly. *Proc*
582 *Natl Acad Sci U S A* 108:15822-7.
- 583 14. Goffin C, Ghuysen JM. 1998. Multimodular penicillin-binding proteins: an enigmatic
584 family of orthologs and paralogs. *Microbiol Mol Biol Rev* 62:1079-93.
- 585 15. Sauvage E, Kerff F, Terrak M, Ayala JA, Charlier P. 2008. The penicillin-binding
586 proteins: structure and role in peptidoglycan biosynthesis. *FEMS Microbiol Rev* 32:234-
587 58.

- 588 16. Vigouroux A, Cordier B, Aristov A, Alvarez L, Ozbaykal G, Chaze T, Oldewurtel ER,
589 Matondo M, Cava F, Bikard D, van Teeffelen S. 2020. Class-A penicillin binding
590 proteins do not contribute to cell shape but repair cell-wall defects. *Elife* 9.
- 591 17. Mueller EA, Egan AJ, Breukink E, Vollmer W, Levin PA. 2019. Plasticity of *Escherichia*
592 *coli* cell wall metabolism promotes fitness and antibiotic resistance across environmental
593 conditions. *Elife* 8.
- 594 18. Paradis-Bleau C, Markovski M, Uehara T, Lupoli TJ, Walker S, Kahne DE, Bernhardt
595 TG. 2010. Lipoprotein cofactors located in the outer membrane activate bacterial cell
596 wall polymerases. *Cell* 143:1110-20.
- 597 19. Typas A, Banzhaf M, van den Berg van Saparoea B, Verheul J, Biboy J, Nichols RJ,
598 Zietek M, Beilharz K, Kannenberg K, von Rechenberg M, Breukink E, den Blaauwen T,
599 Gross CA, Vollmer W. 2010. Regulation of peptidoglycan synthesis by outer-membrane
600 proteins. *Cell* 143:1097-109.
- 601 20. Greene NG, Fumeaux C, Bernhardt TG. 2018. Conserved mechanism of cell-wall
602 synthase regulation revealed by the identification of a new PBP activator in *Pseudomonas*
603 *aeruginosa*. *Proc Natl Acad Sci U S A* 115:3150-3155.
- 604 21. Murphy SG, Murtha AN, Zhao Z, Alvarez L, Diebold P, Shin JH, VanNieuwenhze MS,
605 Cava F, Dorr T. 2021. Class A Penicillin-Binding Protein-Mediated Cell Wall Synthesis
606 Promotes Structural Integrity during Peptidoglycan Endopeptidase Insufficiency in
607 *Vibrio cholerae*. *mBio* 12.
- 608 22. Dersch S, Mehl J, Stuckenschneider L, Mayer B, Roth J, Rohrbach A, Graumann PL.
609 2020. Super-Resolution Microscopy and Single-Molecule Tracking Reveal Distinct
610 Adaptive Dynamics of MreB and of Cell Wall-Synthesis Enzymes. *Front Microbiol*
611 11:1946.
- 612 23. Billaudeau C, Chastanet A, Yao Z, Cornilleau C, Mirouze N, Fromion V, Carballido-
613 Lopez R. 2017. Contrasting mechanisms of growth in two model rod-shaped bacteria.
614 *Nat Commun* 8:15370.
- 615 24. Wamp S RP, Holland G, Halbedel S. 2021. MurA escape mutations uncouple
616 peptidoglycan biosynthesis from PrkA signaling. *bioRxiv preprint*
617 doi:<https://doi.org/10.1101/2021.09.09.459578>
- 618 .
- 619 25. Henrichfreise B, Brunke M, Viollier PH. 2016. Bacterial Surfaces: The Wall that SEDS
620 Built. *Curr Biol* 26:R1158-R1160.
- 621 26. Otten C, Brilll M, Vollmer W, Viollier PH, Salje J. 2018. Peptidoglycan in obligate
622 intracellular bacteria. *Mol Microbiol* 107:142-163.
- 623 27. Atwal S, Chuenklin S, Bonder EM, Flores J, Gillespie JJ, Driscoll TP, Salje J. 2021.
624 Discovery of a Diverse Set of Bacteria That Build Their Cell Walls without the Canonical
625 Peptidoglycan Polymerase aPBP. *mBio* 12:e0134221.
- 626 28. Williams MA, Aliashkevich A, Krol E, Kuru E, Bouchier JM, Rittichier J, Brun YV,
627 VanNieuwenhze MS, Becker A, Cava F, Brown PJB. 2021. Unipolar Peptidoglycan
628 Synthesis in the Rhizobiales Requires an Essential Class A Penicillin-Binding Protein.
629 *mBio* doi:10.1128/mBio.02346-21:e0234621.
- 630 29. Arora D, Chawla Y, Malakar B, Singh A, Nandicoori VK. 2018. The transpeptidase
631 PbpA and noncanonical transglycosylase RodA of *Mycobacterium tuberculosis* play
632 important roles in regulating bacterial cell lengths. *J Biol Chem* 293:6497-6516.
- 633 30. Cole ST. 1998. Comparative mycobacterial genomics. *Curr Opin Microbiol* 1:567-71.

- 634 31. Sher JW, Lim HC, Bernhardt TG. 2021. Polar Growth in *Corynebacterium glutamicum*
635 Has a Flexible Cell Wall Synthase Requirement. *mBio* 12:e0068221.
- 636 32. Sasseti CM, Rubin EJ. 2003. Genetic requirements for mycobacterial survival during
637 infection. *Proc Natl Acad Sci U S A* 100:12989-94.
- 638 33. Dragset MS, Ioerger TR, Zhang YJ, Maerk M, Ginbot Z, Sacchettini JC, Flo TH, Rubin
639 EJ, Steigedal M. 2019. Genome-wide Phenotypic Profiling Identifies and Categorizes
640 Genes Required for Mycobacterial Low Iron Fitness. *Sci Rep* 9:11394.
- 641 34. Hett EC, Chao MC, Rubin EJ. 2010. Interaction and modulation of two antagonistic cell
642 wall enzymes of mycobacteria. *PLoS Pathog* 6:e1001020.
- 643 35. Vandal OH, Roberts JA, Odaira T, Schnappinger D, Nathan CF, Ehrt S. 2009. Acid-
644 susceptible mutants of *Mycobacterium tuberculosis* share hypersusceptibility to cell wall
645 and oxidative stress and to the host environment. *J Bacteriol* 191:625-31.
- 646 36. Smith CM, Richard E. Baker, Megan K. Proulx, Bibhuti B. Mishra, Jarukit E. Long, Sae
647 Woong Park, Ha-Na Lee, VMichael C. Kiritsy, Michelle M. Bellerose, Andrew J. Olive,
648 Kenan C. Murphy, Kadamba Papavinasasundaram, Frederick J. Boehm, Charlotte J.
649 Reames, Rachel K. Meade, Brea K. Hampton, Colton L. Linnertz, Ginger D. Shaw, Pablo
650 Hock, Timothy A. Bell, View Sabine Ehrt, Dirk Schnappinger, Fernando Pardo-Manuel
651 de Villena, Martin T. Ferris, Thomas R. Ioerger, Christopher M. Sasseti. 2021. Host-
652 pathogen genetic interactions underlie tuberculosis susceptibility. *bioRxiv preprint*
653 doi:<https://doi.org/10.1101/2020.12.01.405514>.
- 654 37. Zhang YJ, Reddy MC, Ioerger TR, Rothchild AC, Dartois V, Schuster BM, Trauner A,
655 Wallis D, Galaviz S, Huttenhower C, Sacchettini JC, Behar SM, Rubin EJ. 2013.
656 Tryptophan biosynthesis protects mycobacteria from CD4 T-cell-mediated killing. *Cell*
657 155:1296-308.
- 658 38. Kieser KJ, Boutte CC, Kester JC, Baer CE, Barczak AK, Meniche X, Chao MC, Rego
659 EH, Sasseti CM, Fortune SM, Rubin EJ. 2015. Phosphorylation of the Peptidoglycan
660 Synthase PonA1 Governs the Rate of Polar Elongation in Mycobacteria. *PLoS Pathog*
661 11:e1005010.
- 662 39. Rengarajan J, Bloom BR, Rubin EJ. 2005. Genome-wide requirements for
663 *Mycobacterium tuberculosis* adaptation and survival in macrophages. *Proc Natl Acad Sci*
664 *U S A* 102:8327-32.
- 665 40. Garcia-Heredia A, Pohane AA, Melzer ES, Carr CR, Fiolek TJ, Rundell SR, Lim HC,
666 Wagner JC, Morita YS, Swarts BM, Siegrist MS. 2018. Peptidoglycan precursor
667 synthesis along the sidewall of pole-growing mycobacteria. *Elife* 7.
- 668 41. Daitch AK, Goley ED. 2020. Uncovering Unappreciated Activities and Niche Functions
669 of Bacterial Cell Wall Enzymes. *Curr Biol* 30:R1170-R1175.
- 670 42. Dion MF, Kapoor M, Sun Y, Wilson S, Ryan J, Vigouroux A, van Teeffelen S,
671 Oldenbourg R, Garner EC. 2019. *Bacillus subtilis* cell diameter is determined by the
672 opposing actions of two distinct cell wall synthetic systems. *Nat Microbiol* 4:1294-1305.
- 673 43. Garcia-Heredia A, Kado T, Sein CE, Puffal J, Osman SH, Judd J, Gray TA, Morita YS,
674 Siegrist MS. 2021. Membrane-partitioned cell wall synthesis in mycobacteria. *Elife* 10.
- 675 44. Baranowski C, Welsh MA, Sham LT, Eskandarian HA, Lim HC, Kieser KJ, Wagner JC,
676 McKinney JD, Fantner GE, Ioerger TR, Walker S, Bernhardt TG, Rubin EJ, Rego EH.
677 2018. Maturing *Mycobacterium smegmatis* peptidoglycan requires non-canonical
678 crosslinks to maintain shape. *Elife* 7.

- 679 45. Harrison J, Lloyd G, Joe M, Lowary TL, Reynolds E, Walters-Morgan H, Bhatt A,
680 Lovering A, Besra GS, Alderwick LJ. 2016. Lcp1 Is a Phosphotransferase Responsible
681 for Ligating Arabinogalactan to Peptidoglycan in *Mycobacterium tuberculosis*. *mBio* 7.
682 46. Belisle JT, Vissa VD, Sievert T, Takayama K, Brennan PJ, Besra GS. 1997. Role of the
683 major antigen of *Mycobacterium tuberculosis* in cell wall biogenesis. *Science* 276:1420-
684 2.
- 685 47. Aldridge BB, Fernandez-Suarez M, Heller D, Ambravaneswaran V, Irimia D, Toner M,
686 Fortune SM. 2012. Asymmetry and aging of mycobacterial cells lead to variable growth
687 and antibiotic susceptibility. *Science* 335:100-4.
- 688 48. Botella H, Yang G, Ouerfelli O, Ehrt S, Nathan CF, Vaubourgeix J. 2017. Distinct
689 Spatiotemporal Dynamics of Peptidoglycan Synthesis between *Mycobacterium*
690 *smegmatis* and *Mycobacterium tuberculosis*. *MBio* 8.
- 691 49. Joyce G, Williams KJ, Robb M, Noens E, Tizzano B, Shahrezaei V, Robertson BD. 2012.
692 Cell division site placement and asymmetric growth in mycobacteria. *PLoS One*
693 7:e44582.
- 694 50. Meniche X, Otten R, Siegrist MS, Baer CE, Murphy KC, Bertozzi CR, Sasseti CM.
695 2014. Subpolar addition of new cell wall is directed by DivIVA in mycobacteria. *Proc*
696 *Natl Acad Sci U S A* 111:E3243-51.
- 697 51. Rego EH, Audette RE, Rubin EJ. 2017. Deletion of a mycobacterial divisome factor
698 collapses single-cell phenotypic heterogeneity. *Nature* 546:153-157.
- 699 52. Singh B, Nitharwal RG, Ramesh M, Pettersson BM, Kirsebom LA, Dasgupta S. 2013.
700 Asymmetric growth and division in *Mycobacterium* spp.: compensatory mechanisms for
701 non-medial septa. *Mol Microbiol* 88:64-76.
- 702 53. Liechti GW, Kuru E, Hall E, Kalinda A, Brun YV, VanNieuwenhze M, Maurelli AT.
703 2014. A new metabolic cell-wall labelling method reveals peptidoglycan in *Chlamydia*
704 *trachomatis*. *Nature* 506:507-10.
- 705 54. Sarkar S, Libby EA, Pidgeon SE, Dworkin J, Pires MM. 2016. In Vivo Probe of Lipid II-
706 Interacting Proteins. *Angew Chem Int Ed Engl* 55:8401-4.
- 707 55. Welzel P. 2005. Syntheses around the transglycosylation step in peptidoglycan
708 biosynthesis. *Chem Rev* 105:4610-60.
- 709 56. Gampe CM, Tsukamoto H, Doud EH, Walker S, Kahne D. 2013. Tuning the
710 moenomycin pharmacophore to enable discovery of bacterial cell wall synthesis
711 inhibitors. *J Am Chem Soc* 135:3776-9.
- 712 57. Ostash B, Walker S. 2010. Moenomycin family antibiotics: chemical synthesis,
713 biosynthesis, and biological activity. *Nat Prod Rep* 27:1594-617.
- 714 58. Rebets Y, Lupoli T, Qiao Y, Schirner K, Villet R, Hooper D, Kahne D, Walker S. 2014.
715 Moenomycin resistance mutations in *Staphylococcus aureus* reduce peptidoglycan chain
716 length and cause aberrant cell division. *ACS Chem Biol* 9:459-67.
- 717 59. Yang S, Zhang F, Kang J, Zhang W, Deng G, Xin Y, Ma Y. 2014. *Mycobacterium*
718 *tuberculosis* Rv1096 protein: gene cloning, protein expression, and peptidoglycan
719 deacetylase activity. *BMC Microbiol* 14:174.
- 720 60. Kang CM, Nyayapathy S, Lee JY, Suh JW, Husson RN. 2008. Wag31, a homologue of
721 the cell division protein DivIVA, regulates growth, morphology and polar cell wall
722 synthesis in mycobacteria. *Microbiology* 154:725-35.
- 723 61. Nguyen L, Scherr N, Gatfield J, Walburger A, Pieters J, Thompson CJ. 2007. Antigen 84,
724 an effector of pleiomorphism in *Mycobacterium smegmatis*. *J Bacteriol* 189:7896-910.

- 725 62. Melzer ES, Sein CE, Chambers JJ, Sloan Siegrist M. 2018. DivIVA concentrates
726 mycobacterial cell envelope assembly for initiation and stabilization of polar growth.
727 Cytoskeleton (Hoboken) 75:498-507.
- 728 63. Thanky NR, You
729
- 730 ng DB, Robertson BD. 2007. Unusual features of the cell cycle in mycobacteria: polar-restricted
731 growth and the snapping-model of cell division. Tuberculosis (Edinb) 87:231-6.
- 732 64. Pidgeon SE, Apostolos AJ, Nelson JM, Shaku M, Rimal B, Islam MN, Crick DC, Kim
733 SJ, Pavelka MS, Kana BD, Pires MM. 2019. L,D-Transpeptidase Specific Probe Reveals
734 Spatial Activity of Peptidoglycan Cross-Linking. ACS Chem Biol 14:2185-2196.
- 735 65. Monteiro JM, Pereira AR, Reichmann NT, Saraiva BM, Fernandes PB, Veiga H, Tavares
736 AC, Santos M, Ferreira MT, Macario V, VanNieuwenhze MS, Filipe SR, Pinho MG.
737 2018. Peptidoglycan synthesis drives an FtsZ-treadmilling-independent step of
738 cytokinesis. Nature 554:528-532.
- 739 66. Rismondo J, Halbedel S, Grundling A. 2019. Cell Shape and Antibiotic Resistance Are
740 Maintained by the Activity of Multiple FtsW and RodA Enzymes in *Listeria*
741 *monocytogenes*. mBio 10.
- 742 67. Siegrist MS, Swarts BM, Fox DM, Lim SA, Bertozzi CR. 2015. Illumination of growth,
743 division and secretion by metabolic labeling of the bacterial cell surface. FEMS
744 Microbiol Rev 39:184-202.
- 745 68. Siegrist MS, Whiteside S, Jewett JC, Aditham A, Cava F, Bertozzi CR. 2013. (D)-Amino
746 acid chemical reporters reveal peptidoglycan dynamics of an intracellular pathogen. ACS
747 Chem Biol 8:500-5.
- 748 69. Paintdakhi A, Parry B, Campos M, Irnov I, Elf J, Surovtsev I, Jacobs-Wagner C. 2016.
749 Oufi: an integrated software package for high-accuracy, high-throughput quantitative
750 microscopy analysis. Mol Microbiol 99:767-77.
- 751 70. Lord SJ, Velle KB, Mullins RD, Fritz-Laylin LK. 2020. SuperPlots: Communicating
752 reproducibility and variability in cell biology. J Cell Biol 219.
753